Zero–speed sensorless drive capability of fractional–slot inset PM machine

Adriano Faggion Nicola Bianchi Silverio Bolognani
Emanuele Fornasiero

Electric Drives Laboratory
Department of Industrial Engineering
University of Padova

PEMD 2012
Power Electronics, Machines and Drives Conference
Bristol, 27-29 March 2012

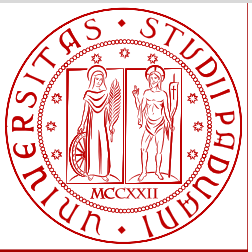

This presentation refers to the paper:

Adriano Faggion, Nicola Bianchi, Silverio Bolognani and Emanuele Fornasiero

”**Zero–speed sensorless drive capability of fractional–slot inset PM machine**”

IEEE – PEMD 2012
Power Electronics, Machines and Drives Conference
Bristol (UK), 27-29 March 2012.

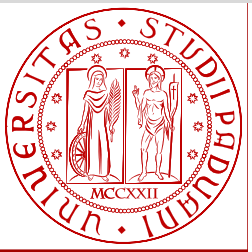

Outline

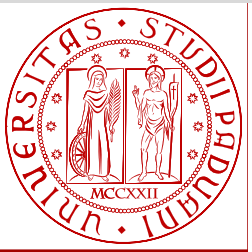

Sensorless control purpose

For the sensorless control purpose, three different rotor configurations are studied in a previous paper:(a) Interior, (b) Ringed–pole and (c) Inset Permanent Magnet (PM) Rotor.

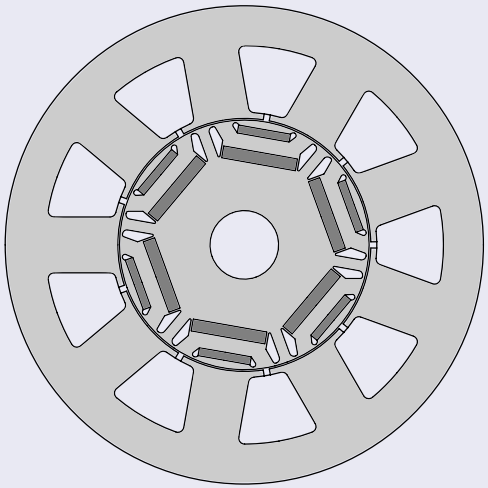

(a) Interior PM motor

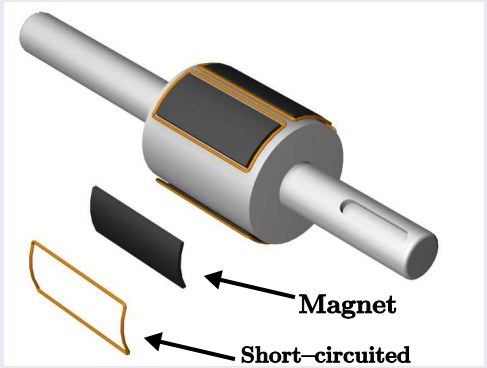

(b) Ringed pole PM Motor

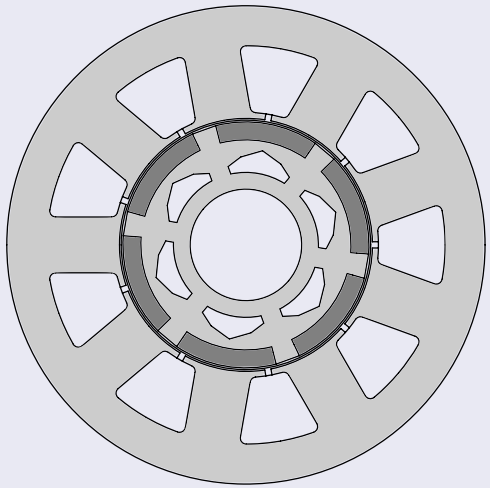

(c) Inset PM motor

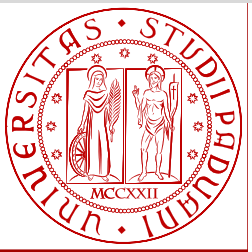

Sensorless control purpose

For the sensorless control purpose, three different rotor configurations are studied in a previous paper:(a) Interior, (b) Ringed–pole and (c) Inset Permanent Magnet (PM) Rotor.

$\Rightarrow$ Among these the inset PM machine results to have a good performance as far as the sensorless rotor position detection is concerned.
Then in the paper a 12–slot 8–pole inset PM configuration is deeply studied.

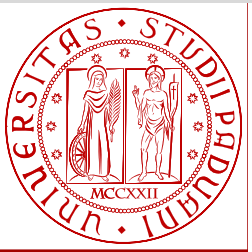

Sensorless technique

1. The detection of the rotor position by means of a high frequency (HF) signal injection is a common sensorless detection technique.
2. It consists on the injection of a HF voltages in the stator windings, which causes a HF currents.
3. HF current vector draws a figure that contains information of the rotor position.

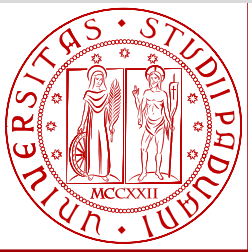

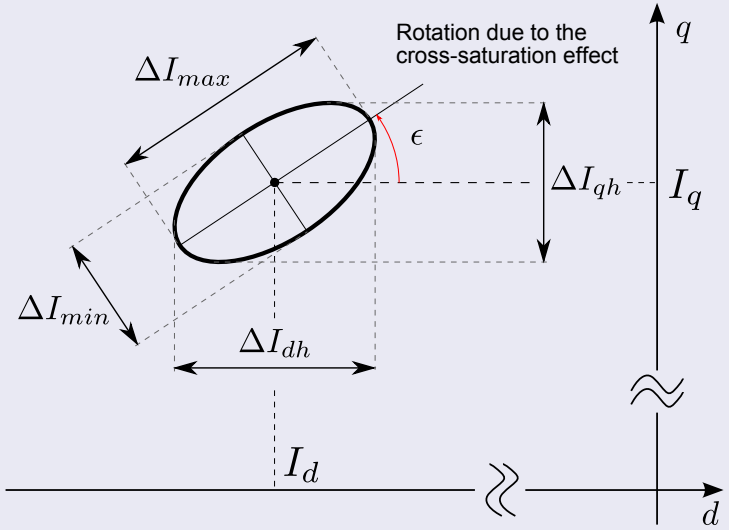

Rotating HF voltage vector

$\Downarrow$

Ellipse HF current vector trajectory

$\Downarrow$

HF saliency can be defined as:

$$\xi_{HF} = \frac{\Delta I_{max}}{\Delta I_{min}}$$

$\Downarrow$

mutual inductance L_{dq_h} causes the ellipse inclination ϵ

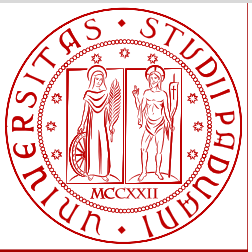

HF rotating voltage, injected in a general rotating reference frame $d^x q^x$, of the type:

$$\begin{aligned} u^x_{d_h} &= U_h cos(\omega_h t) \\ u^x_{q_h} &= U_h sin(\omega_h t) \end{aligned}$$

is adopted.
It is assumed that the machine is standstill (electrical speed equal to zero).

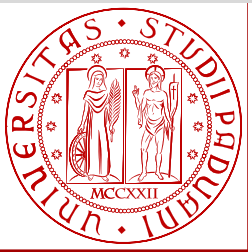

The magnetic model of the machine can be described by means of the matrix of differential HF inductances in each operating point, expressed by:

$$\mathbf{L} = \begin{bmatrix} L_{d_h} & L_{dq_h} \\ L_{qd_h} & L_{q_h} \end{bmatrix}$$

$$L_{avg} = \frac{L_{q_h} + L_{d_h}}{2}$$

$$L_{dif} = \frac{L_{q_h} - L_{d_h}}{2}$$

- L_{d_h} is the HF d–axis inductance
- L_{q_h} is the HF q–axis inductance
- L_{dq_h} is the HF cross saturation inductance
- L_{avg} is the HF average inductance
- L_{dif} is the HF difference inductance.

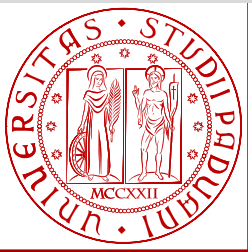

High Frequency current vector results of two components:

$$\bar{i}_{dq_h} = \bar{i}_{cw} + \bar{i}_{ccw}$$

with

$$\begin{aligned} \bar{i}_{cw} &= -\frac{\Lambda_h}{\Delta} L_{avg} e^{j\left(\omega_h t + \frac{\pi}{2}\right)} \\ \bar{i}_{ccw} &= -\frac{\Lambda_h}{\Delta} \sqrt{L_{dif}^2 + L_{dq_h}^2}\, e^{-j\left(2(\Delta\theta - \epsilon) + \omega_h t + \frac{\pi}{2}\right)} \end{aligned}$$

where ϵ is the displacement due to the presence of cross-saturation between the d– and q–axis. It can be computed as:

$$\epsilon = \frac{1}{2} \arctan\left(-\frac{L_{dq_h}}{L_{dif}}\right)$$

and $\Delta = L_{d_h} L_{q_h} - L_{dq_h}^2$,$\Delta\theta = \tilde{\theta}_{me} - \theta_{me}$.

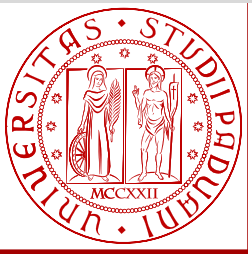

HF voltage vector injection in the actual $dq \Rightarrow \Delta\theta = 0$ and then:

$$\bar{i}_{dq_h} = \underbrace{-\frac{\Lambda_h}{\Delta} L_{avg} e^{j\left(\omega_h t + \frac{\pi}{2}\right)}}_{\bar{i}_{cw}} \underbrace{- \frac{\Lambda_h}{\Delta} \sqrt{L_{dif}^2 + L_{dq_h}^2}\, e^{-j\left(-2\epsilon + \omega_h t + \frac{\pi}{2}\right)}}_{\bar{i}_{ccw}}$$

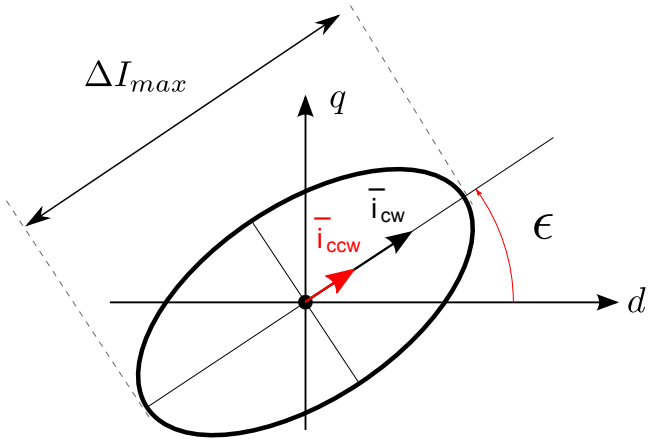

(d)

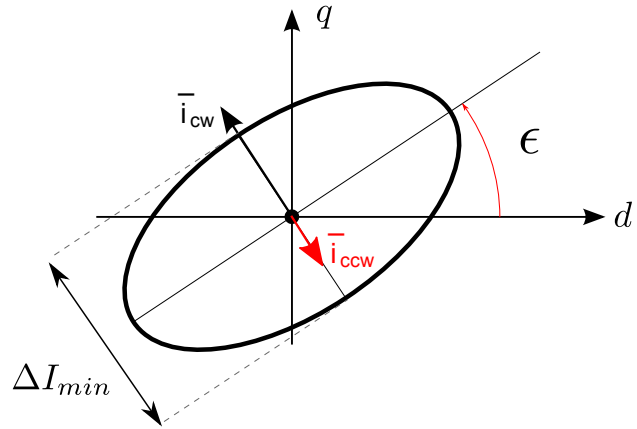

(e)

$$\xi_{HF} = \frac{\Delta I_{max}}{\Delta I_{min}} = \frac{L_{avg} + \sqrt{L_{dif}^2 + L_{dq_h}^2}}{L_{avg} - \sqrt{L_{dif}^2 + L_{dq_h}^2}}$$

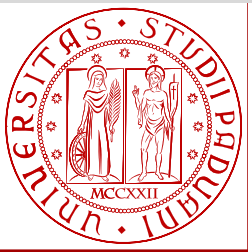

The HF current vector $\bar{i}_{dq_h}$ is used to recognize the maximum axis direction of the ellipse. This should coincide with the *d*–axis.

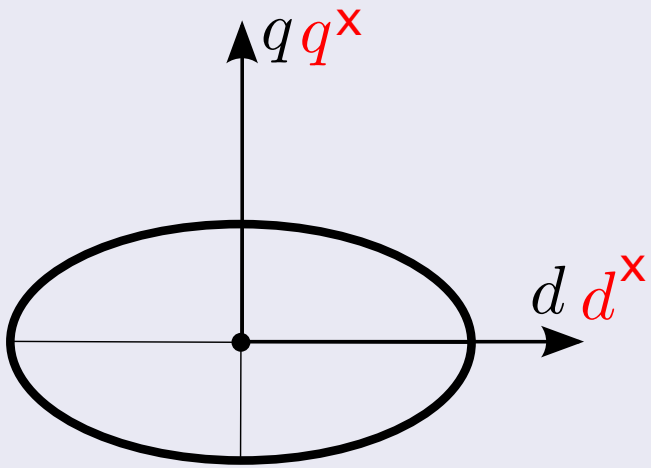

(f) Ideal case $L_{dq_h} = 0$

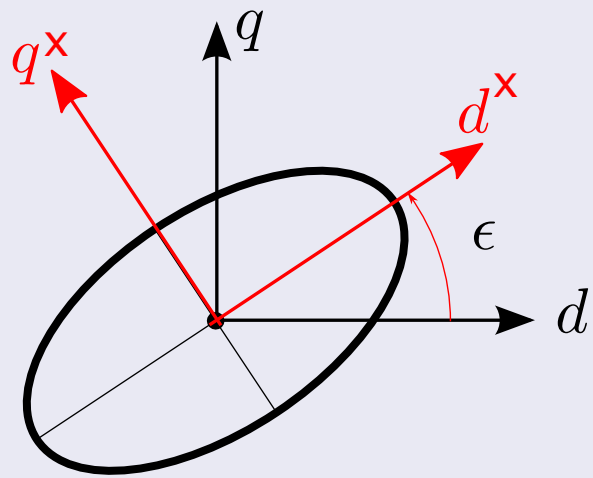

(g) Real case $L_{dq_h} \neq 0$

However, because of the cross–saturation the actual *d*–axis is not correctly recognized but an axis displaced of the angle error ϵ with respect to the *d*–axis is found.

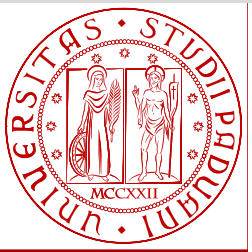

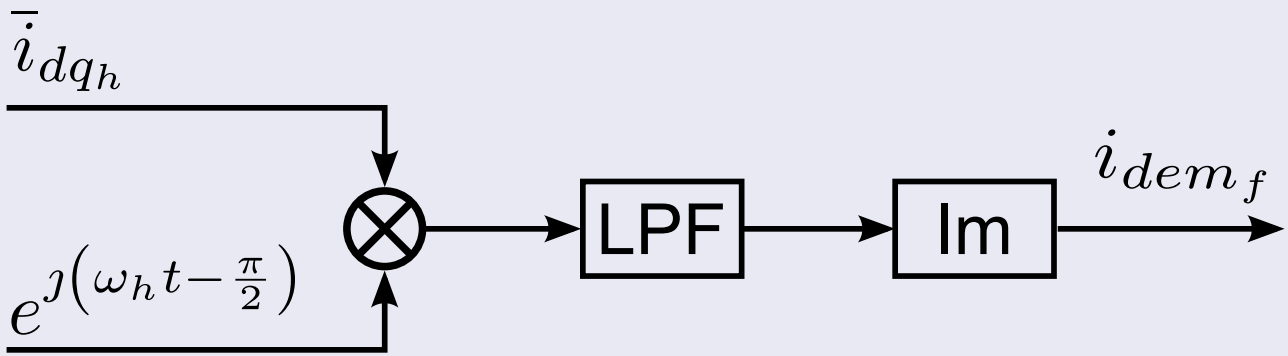

Figure: Sensorless rotor position estimation scheme

Output of the estimation scheme is:

$$i_{dem_f} = -\frac{\Lambda_h}{\Delta}\sqrt{L_{dif}^2 + L_{dq_h}^2}\sin(2\Delta\theta - 2\epsilon)$$

This quantity is manipulated in order to zeroing the term $\Delta\theta - \epsilon$. The result is:

$$\Delta\theta - \epsilon = 0 \quad \Rightarrow \quad \tilde{\theta}_{me} = \theta_{me} + \epsilon$$

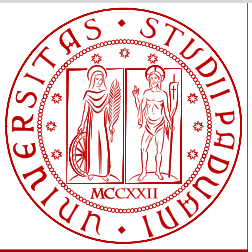

Particular case ♯1

If the motor does not exhibit a cross–saturation between the *d*– and *q*–axis, the angle error ϵ becomes equal to zero. The direction of maximum axis is along the *d*–axis.

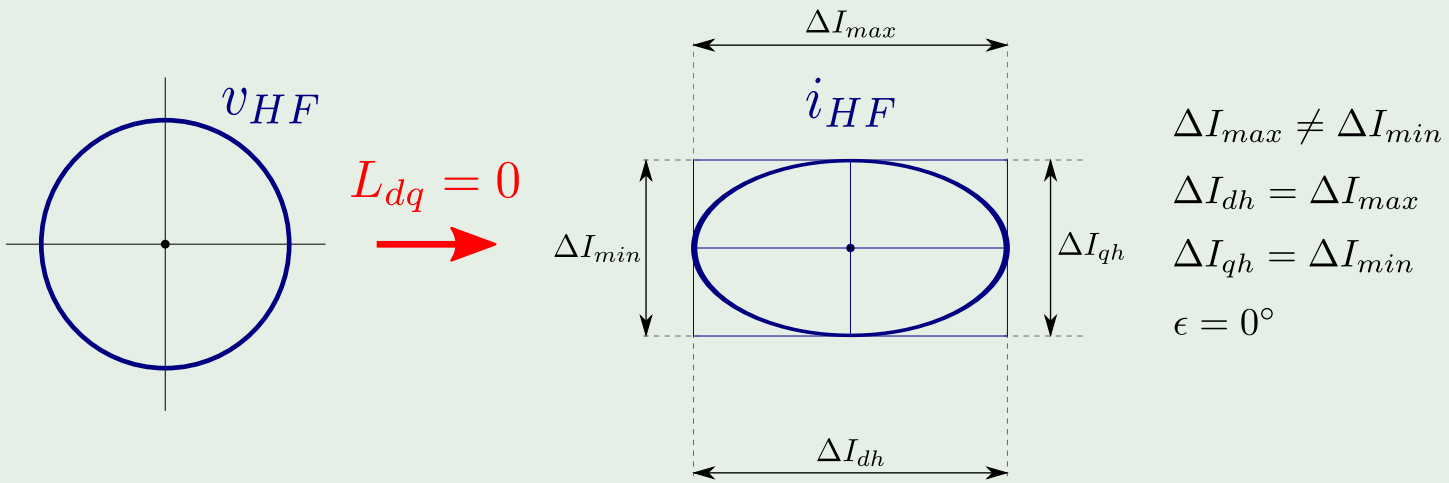

$\Rightarrow$ Correct estimation of the rotor position.

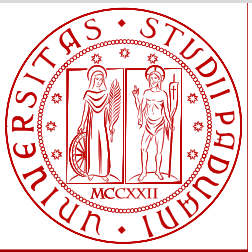

Particular case ♯1

No cross–saturation between the *d*– and *q*–axis. Angle error ϵ becomes zero.

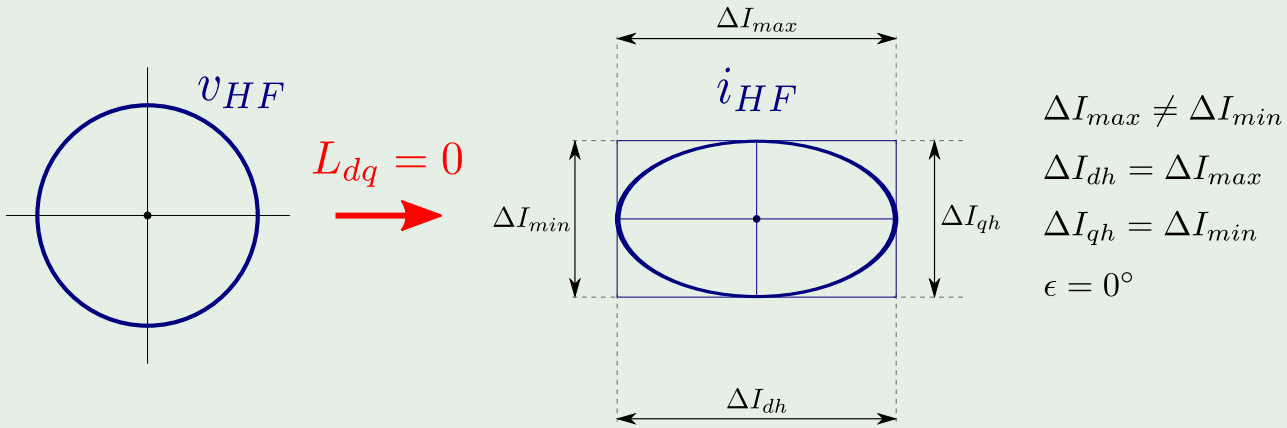

$$\xi_{HF} = \frac{L_{avg} + \sqrt{L_{dif}^2 + L_{dq_h}^2}}{L_{avg} - \sqrt{L_{dif}^2 + L_{dq_h}^2}} \quad \Rightarrow \quad \boxed{\xi_{HF} = \frac{L_{avg} + L_{dif}}{L_{avg} - L_{dif}} = \frac{L_{qh}}{L_{dh}}}$$

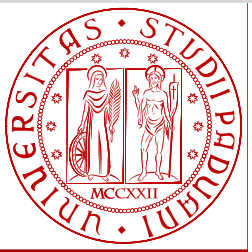

Particular case ♯2

If the *d*– and *q*–axis inductances are equal, the current variation on the *d*– and *q*–axis becomes equal. Anyway, the HF saliency remains, due to the cross-saturation.

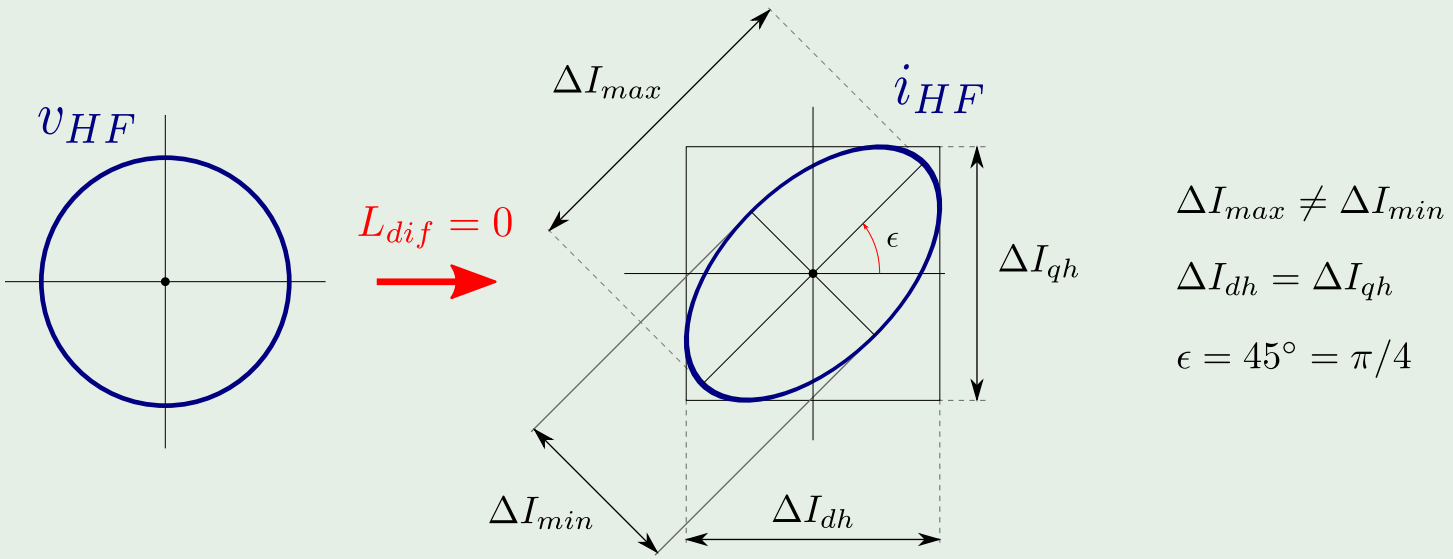

$\Rightarrow$ Rotor position estimation with 45° angle error.

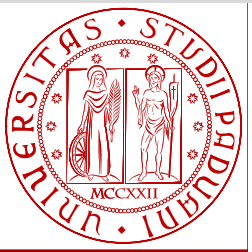

Particular case ♯2

d– and *q*–axis inductances equal. HF saliency remains, due the presence of the cross-saturation.

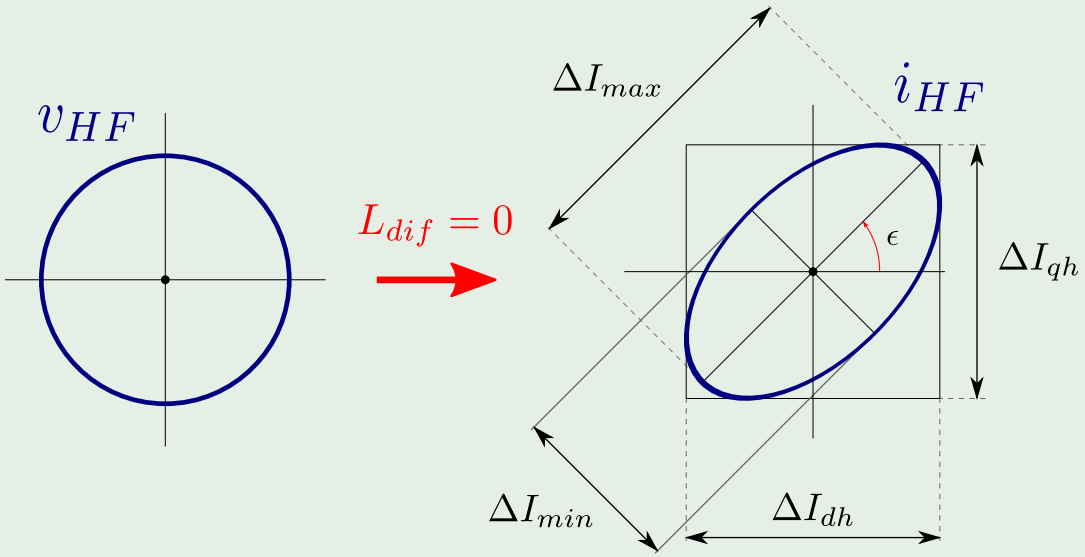

$$\Delta I_{max} \neq \Delta I_{min}$$

$$\Delta I_{dh} = \Delta I_{qh}$$

$$\epsilon = 45° = \pi/4$$

$$\xi_{HF} = \frac{L_{avg} + \sqrt{L_{dif}^2 + L_{dq_h}^2}}{L_{avg} - \sqrt{L_{dif}^2 + L_{dq_h}^2}} \quad \Rightarrow \quad \boxed{\xi_{HF} = \frac{L_{avg} + L_{dq_h}}{L_{avg} - L_{dq_h}}}$$

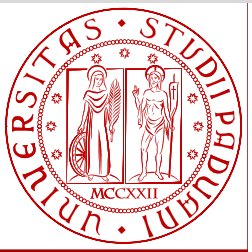

Particular case ♯3

In case of:

- No cross–saturation between the two axes
- *d*– and *q*–axis HF inductances equal

then the current ellipse degenerates into a circle.

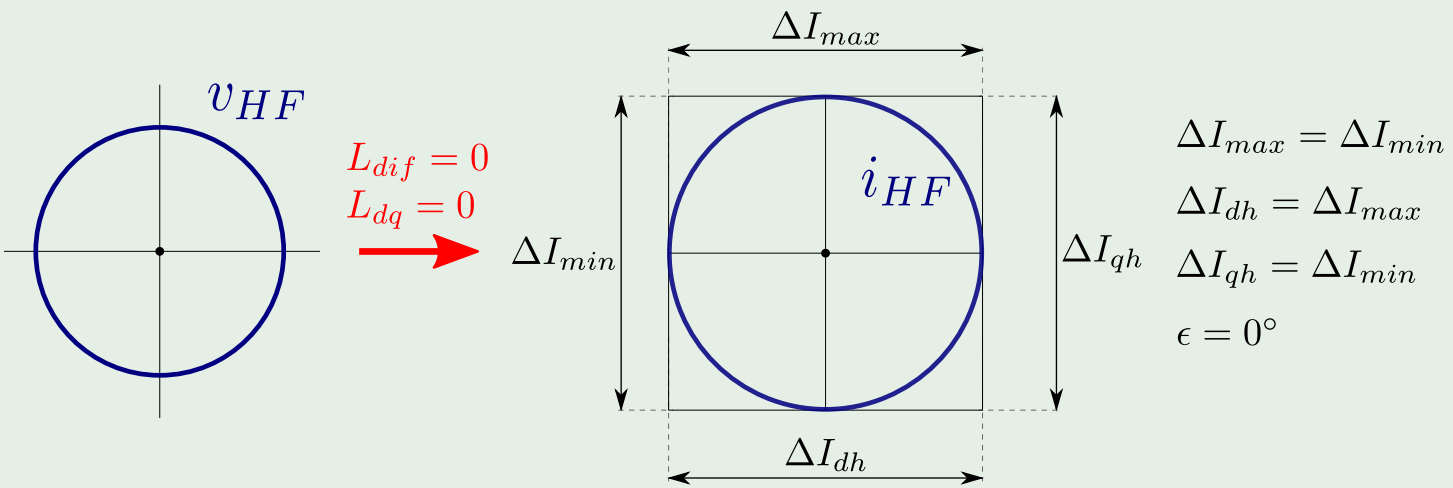

$\Rightarrow$ Rotor position detection not allowable.

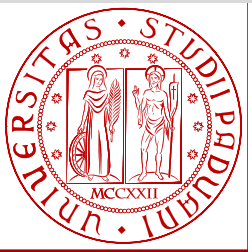

Particular case ♯3

No cross–saturation and *d*– and *q*–axis inductances equal. The current ellipse degenerates in a circumference.

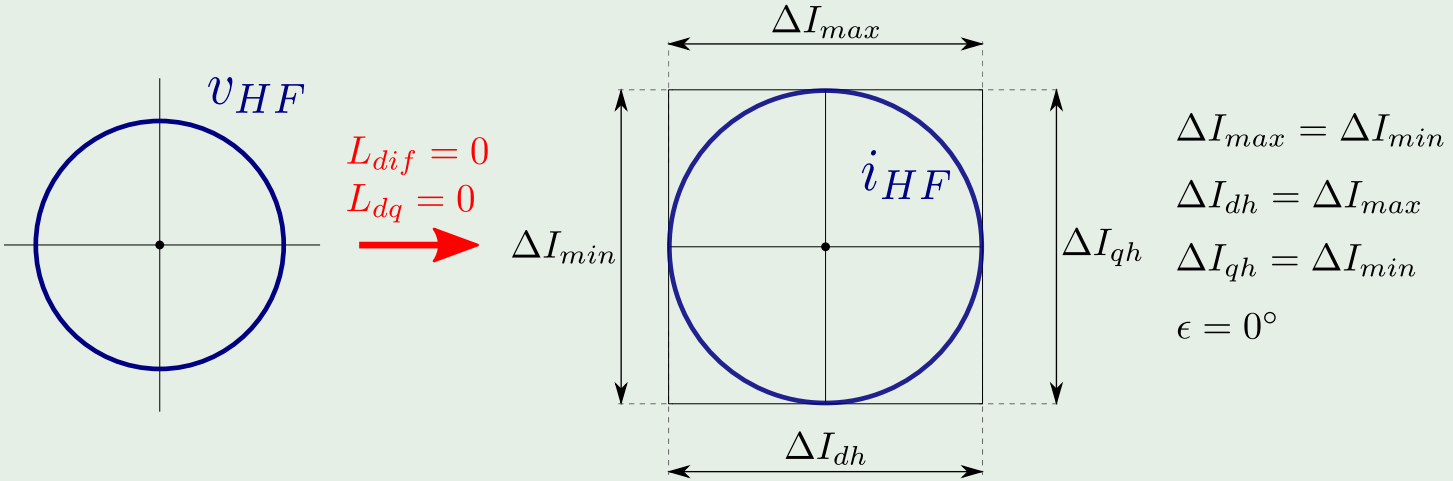

$$\xi_{HF} = \frac{L_{avg} + \sqrt{L_{dif}^2 + L_{dq_h}^2}}{L_{avg} - \sqrt{L_{dif}^2 + L_{dq_h}^2}} \quad \Rightarrow \quad \boxed{\xi_{HF} = \frac{L_{avg}}{L_{avg}} = 1}$$

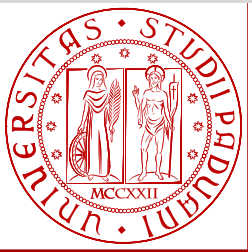

Geometry of 12–slot 8–pole inset PM motor

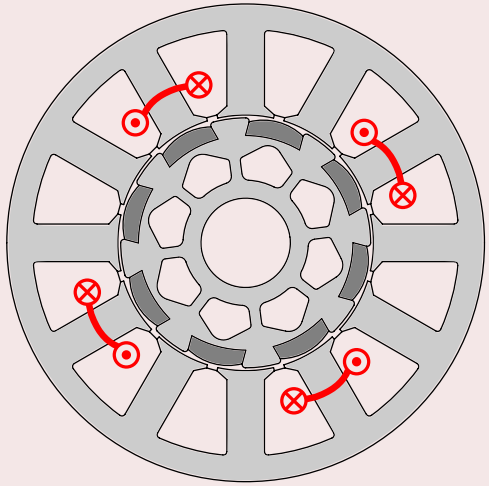

(a)

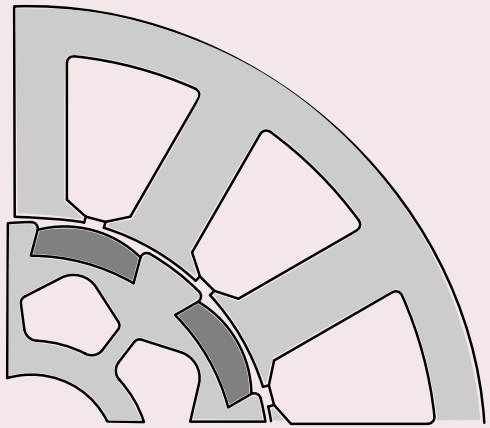

(b)

In red the coil of phase *a*. The stator exhibits a fractional–slot non–overlapped coil winding.

Variable	Dimension	measure unity
Stack length	90	(*mm*)
External stator diameter	133.6	(*mm*)
Inner stator diameter	71.5	(*mm*)
PM thickness	4.95	(*mm*)
PM width	16	(*mm*)

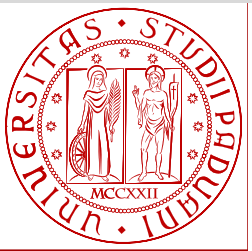

Geometry of 12–slot 8–pole inset PM motor

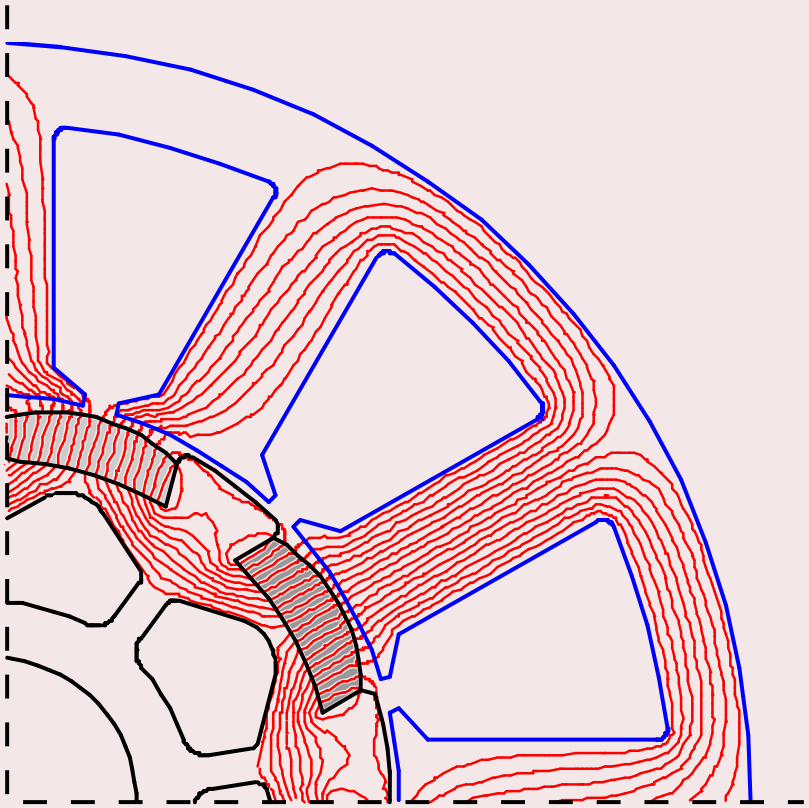

$I_d = 0$ and $I_q = 0$.
Without the current the flux due to the PMs practically doesn't flow through the tooth.

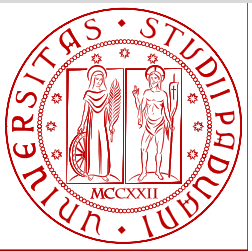

Geometry of 12–slot 8–pole inset PM motor

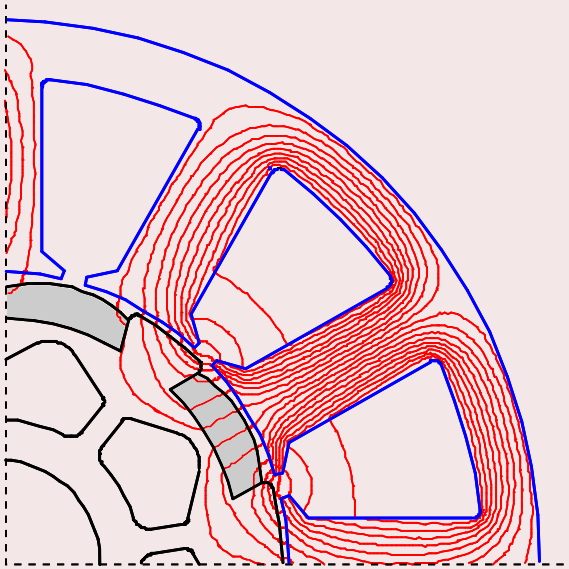

(c) $I_d = I$ and $I_q = 0$

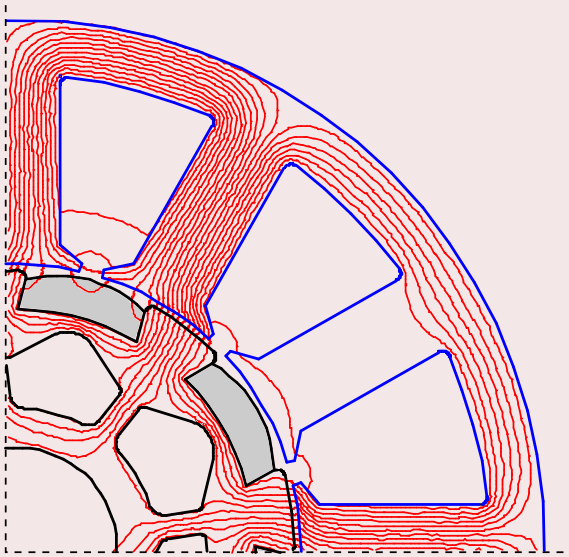

(d) $I_d = 0$ and $I_q = I$

FE simulation have been done excluding the effect of the magnet.
In the case of Fig.(d) there is a more density of the flux lines.
Then the L_q inductance results greater than the L_d one.

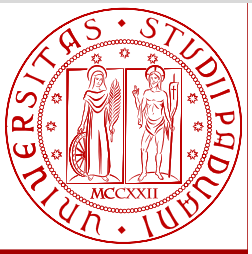

FE Simulations

- The FE simulations have been carried out with the aim of determining the main characteristics of the motor.
- Some simulations have been done for different (I_d, I_q) currents, to cover a wide range of operating points.
- Nominal current is $I_N = 10\ A$.
- The current limits are $-20\ A \leq I_d \leq 20\ A$ and $0\ A \leq I_q \leq 20\ A$.
- The differential inductances are computed and the magnetic saliency of the motor is derived.

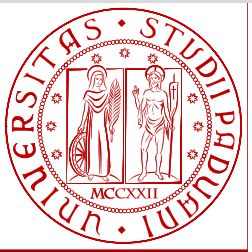

Map of the magnetic saliency ξ_{HF}

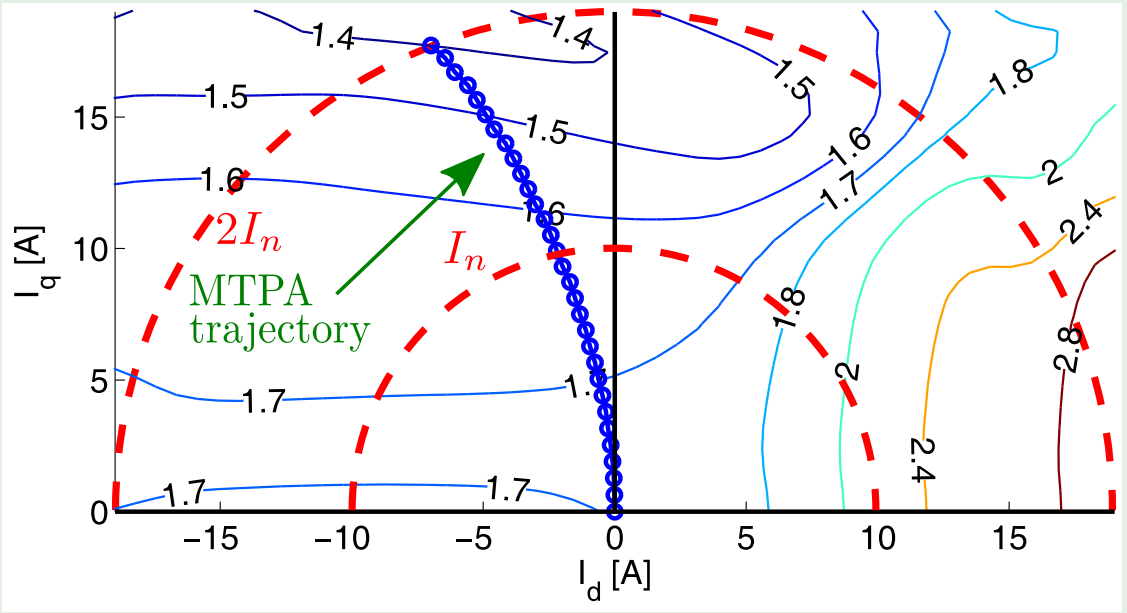

- **It is worth noticing that the saliency is sufficiently high in the whole second half plane. It remains around** $\xi_{HF} = 1.6$**.**

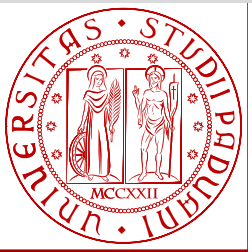

Map of the ratio L_{dif}/L_{avg}.

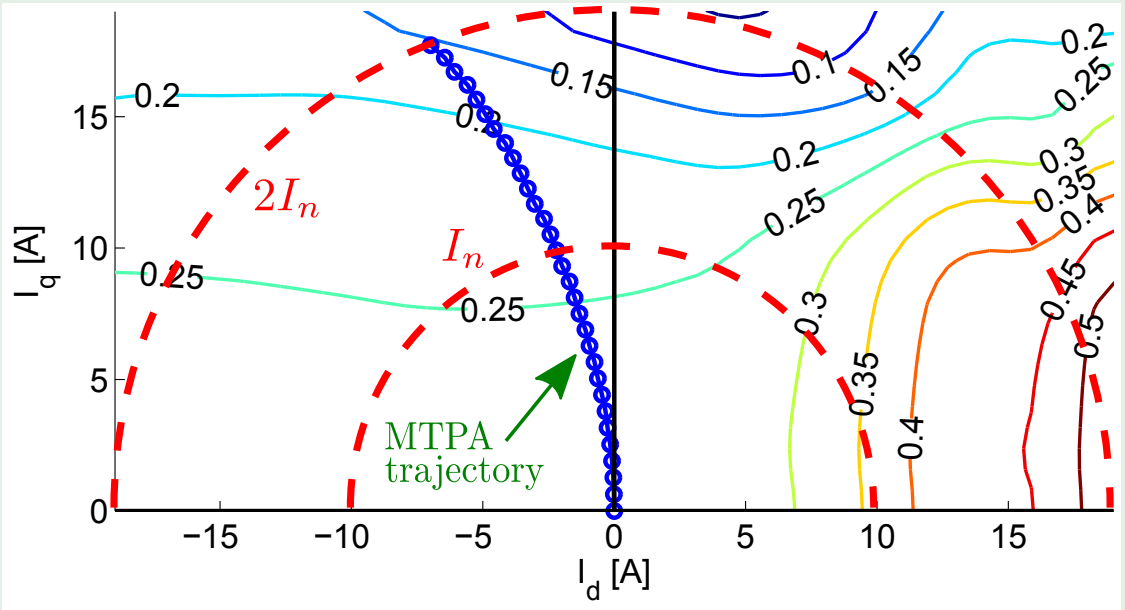

- **The difference inductance L_{dif} is greater than zero in the whole I_d–I_q plane.**

$\Rightarrow$ The rotor position is detected even under overload.

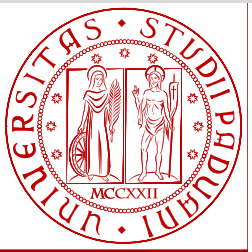

Map of the ratio L_{dq_h}/L_{avg}

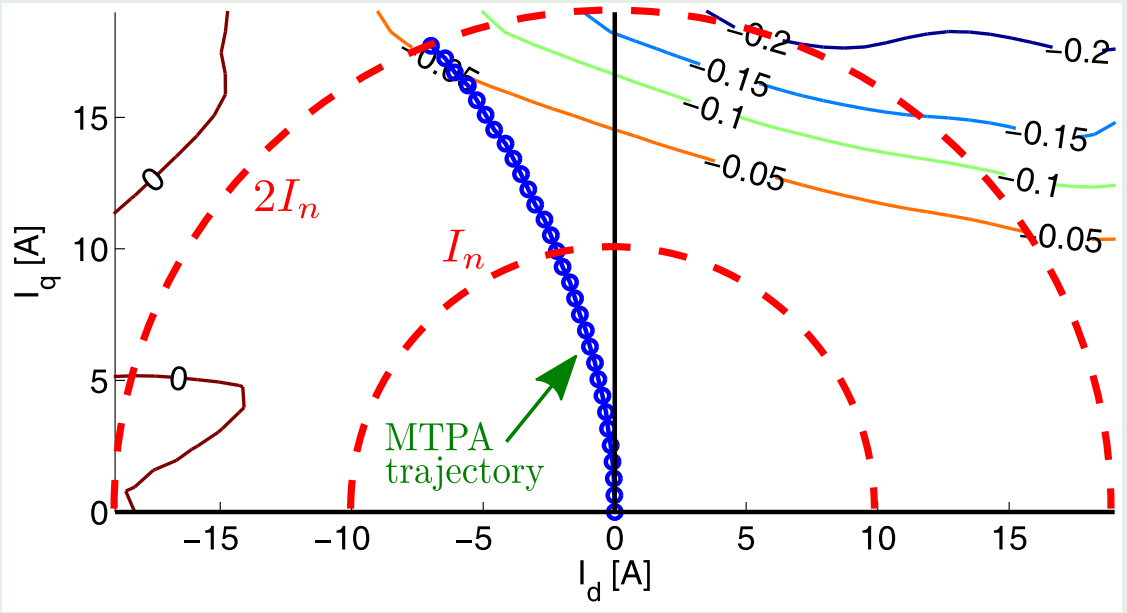

- **The cross–saturation inductance L_{dq_h} is negligible along the MTPA trajectory.**

$\Rightarrow$ The angle error ϵ is very low.

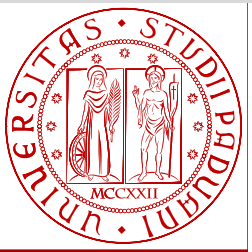

Map of the error $|\epsilon|$ due to cross–coupling (deg)

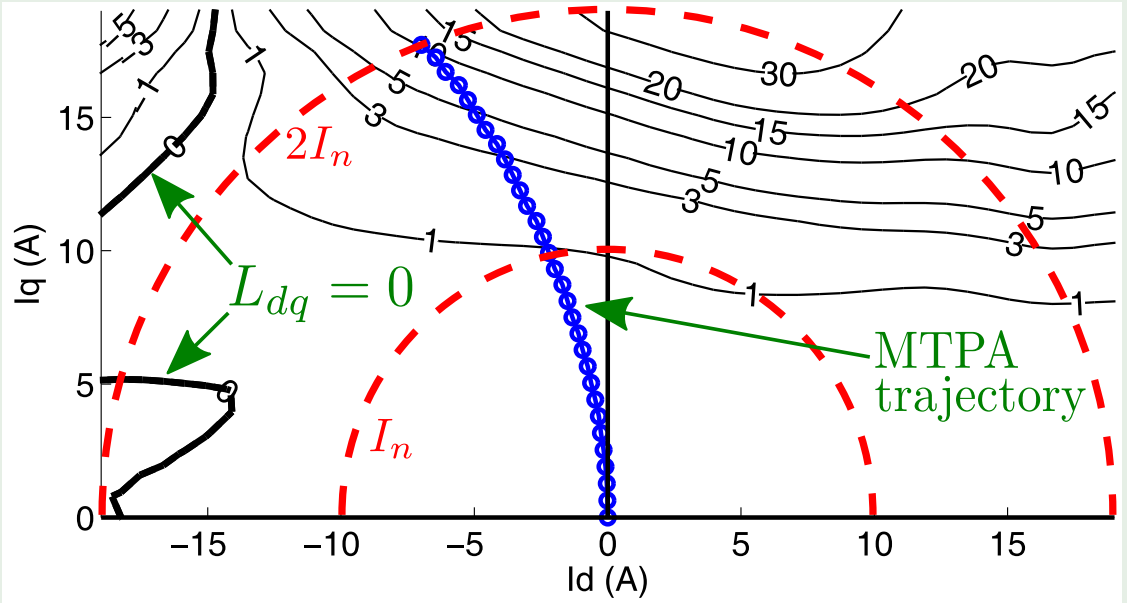

- ϵ **remains lower than** 1 *el.deg.* **up to the nominal current.**
- ϵ **increases for higher currents, however remaining lower than** 10 *el.deg.* **along the MTPA trajectory.**

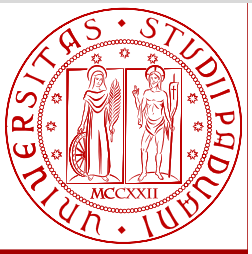

Inset 12–slot 8–pole rotor configuration

Summary of the motor characteristics

- ✓ A difference inductance L_{dif} is always greater than zero in a whole plane, since $L_{qh} > L_{dh}$.
- ✓ The mutual differential inductance is negligible, since it is quite similar to that on a SPM motor.
- ✓ The angle error due to the cross–saturation is very low, especially along the MTPA trajectory.

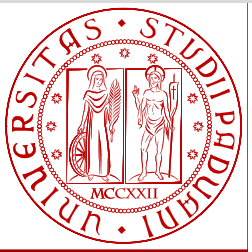

Test bench setup

Some experimental tests have been carried out in order to verify the self–sensing motor capability in all the *dq* current plane.

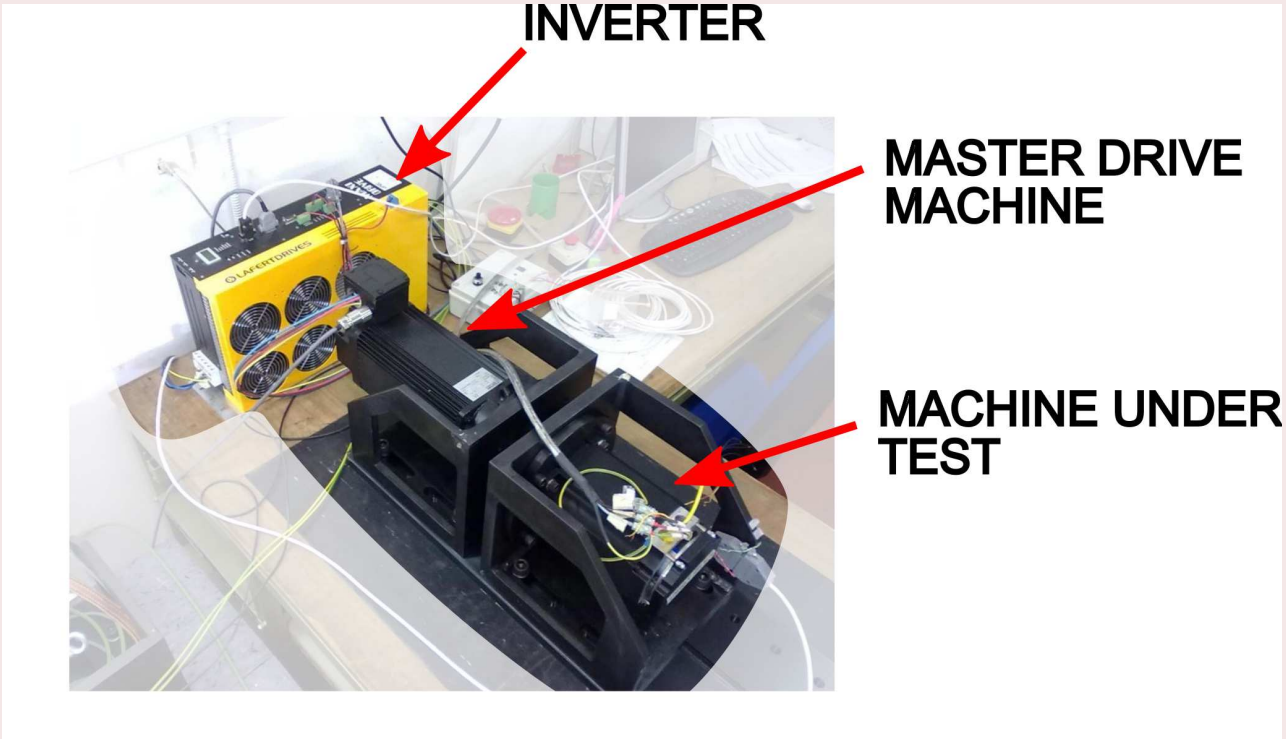

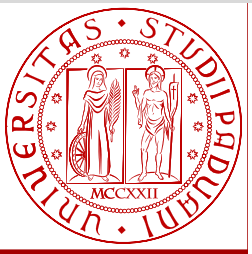

Experimental setup

- The machine under test is coupled to a master drive.
- The master drive can be speed– or torque–controlled by an industrial inverter.
- The inset PM machine is controlled by a laboratory inverter monitored by an acquisition system.
- A rotating voltage vector, with amplitude U_h equal to 20 V, is added to the reference power voltages u_d^* and u_q^* given by the current regulators.
- The injection frequency is set to 500 Hz.
- The tests have been carried out locking the inset PM machine by the master one.

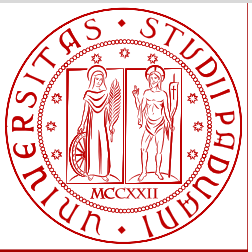

High frequency currents at two different working points along the MTPA trajectory

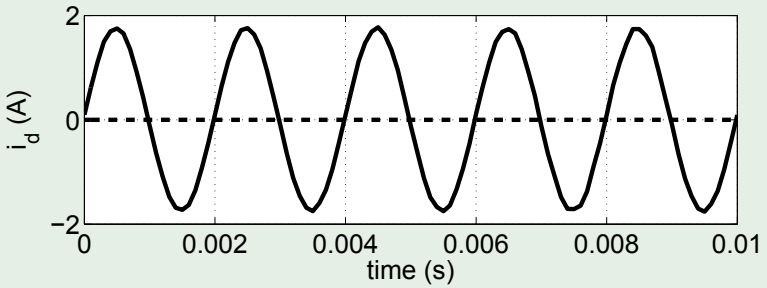

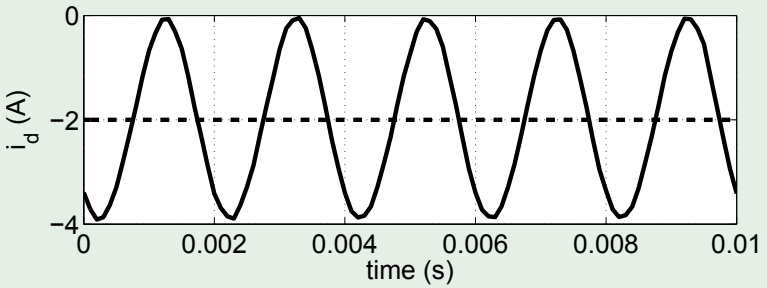

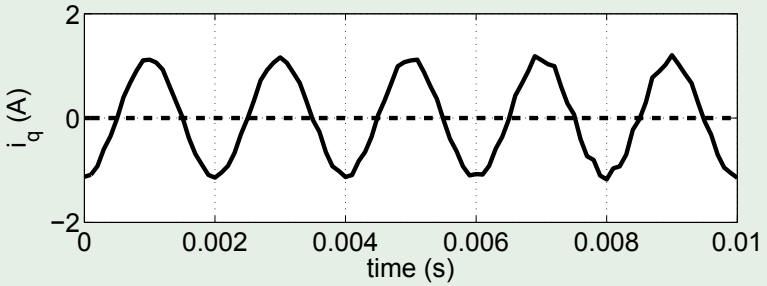

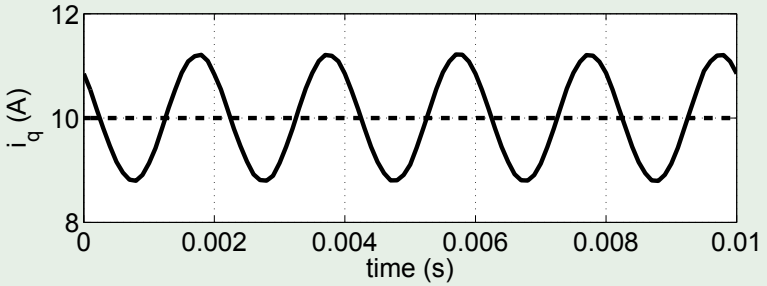

(e) $i_d = 0$ and $i_q = 0$

(f) $i_d = -2$ and $i_q = 10$

✓ Each current is given by the sum of a constant value and a sinusoidal signal due to the HF voltage injection.
✓ The amplitude of the i_q current oscillation is lower than that of the i_d current, being $L_{q_h} > L_{d_h}$.

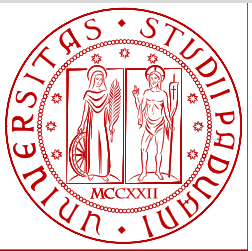

High frequency ellipses in the i_d–i_q plane

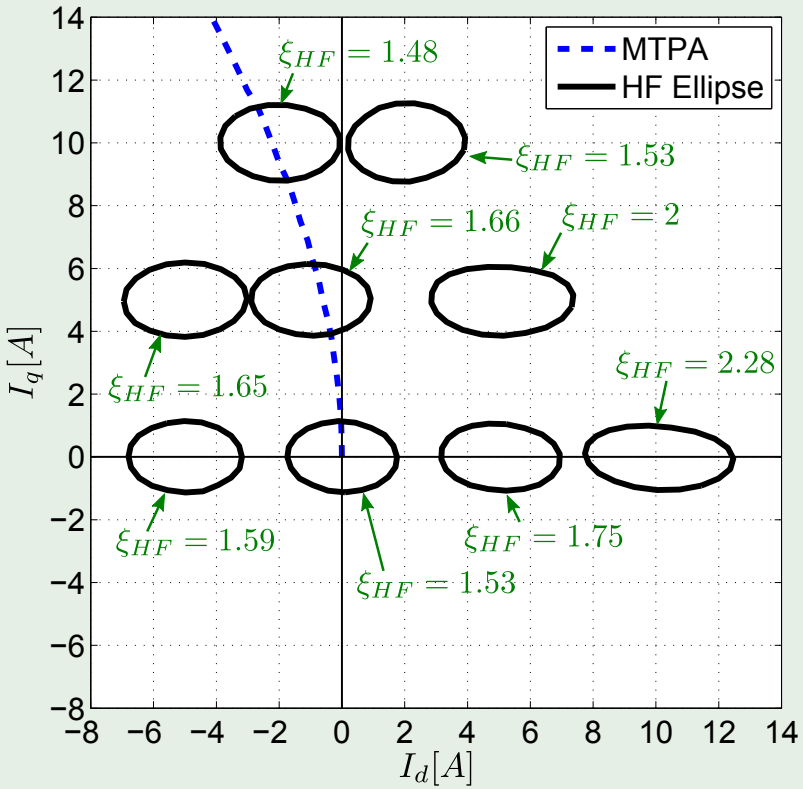

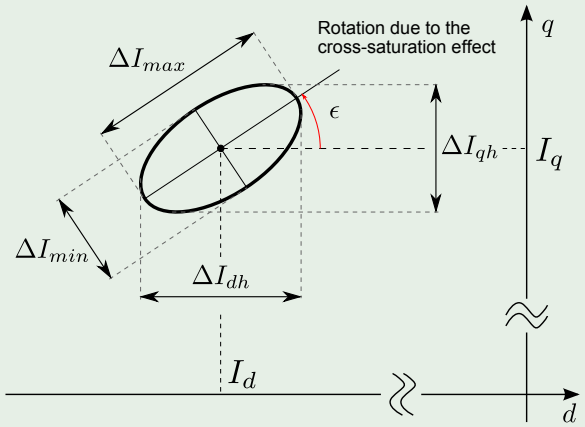

✓ The HF saliency is obtained applying: $\xi_{hf} = \Delta I_{max}/\Delta I_{min}$.

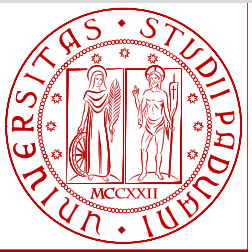

HF Saliency

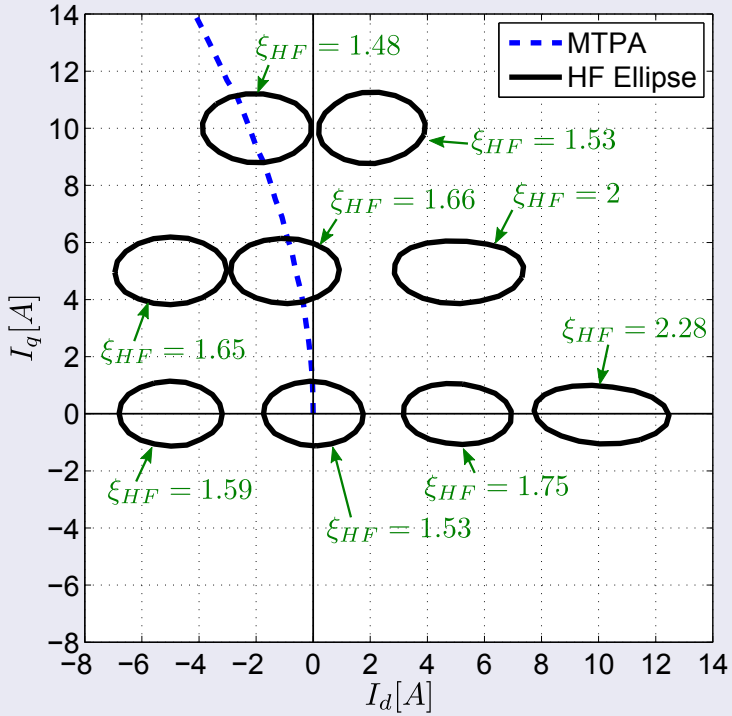

✓ ξ_{HF} for each ellipse are slightly lower to those estimated by FE simulation.

✓ ξ_{HF} remains equal to 1.6 in all the left *dq* half–plane.

✓ FE simulations highlight that the saliency remains also in overload conditions.

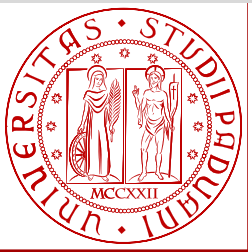

Angle error ϵ

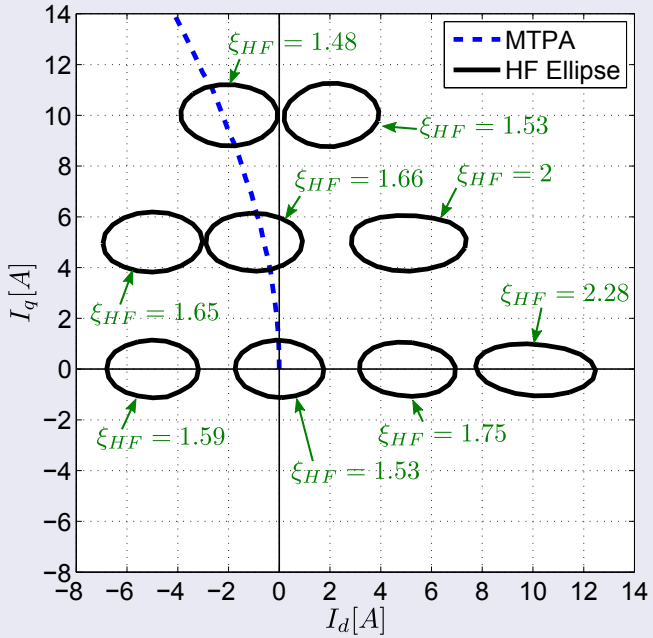

- ✓ All the ellipses have the maximum axis practically parallel to the *d*–axis.
- ✓ This means that the error ϵ is very low.
- ✓ With $|\bar{i}| \leq I_N$ the ϵ remains lower than 1 *el.deg.*.
- ✓ A low error confirms the low cross–saturation effect.
- ✓ This confirms the results given by the FE simulation.

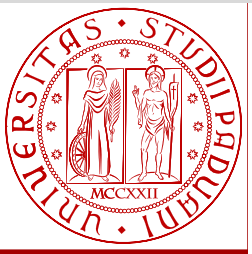

Conclusions

✓ The 12–slot 8–pole inset PM motor results to be very suitable for the sensorless rotor position detection, based on the HF voltage injection.
✓ The iron tooth introduced between each couple of PMs yields a proper HF rotor saliency.
✓ This magnetic behaviour results to be slightly affected by iron saturation and cross–saturation phenomena.
✓ This characteristics remain also under overload operations.

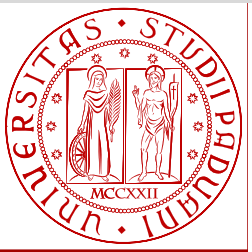

Related Papers by the Authors

S. Bolognani, S. Calligaro, R. Petrella, and M. Tursini, "*Sensorless control of ipm motors in the low–speed range and at stand–still by hf–injection and dft processing.*", In in IEEE International Electric Machines and Drives Conference, 2009. IEMDC '09., May 2009, pp. 1557–1564.

N. Bianchi, S. Bolognani, J.–H. Jang, and S.–K. Sul, "*Advantages of inset pm machines for zero–speed sensorless position detection*", IEEE Trans. on Industry Applications, vol. 44, no. 4, pp. 1190 –1198, 2008.

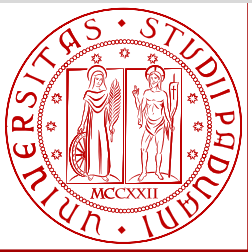

Related Papers by the Authors (cont.)

N. Bianchi, S. Bolognani, and A. Faggion,
"*Predicted and measured errors in estimating rotor position by signal injection for salient-pole pm synchronous motors*",
in IEEE International Electric Machines and Drives Conference, 2009. IEMDC '09., May 2009, pp. 1565–1572.

A. Faggion, S. Bolognani, and N. Bianchi,
"*Ringed–pole permanent magnet synchronous motor for position sensorless drives*",
in IEEE Energy Conversion Congress and Exposition, 2009. ECCE 2009., 2009, pp. 3837 –3844.

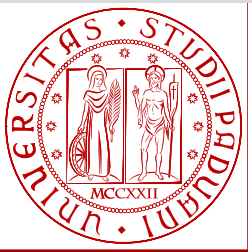

Related Papers by the Authors (cont.)


A. Faggion, N. Bianchi, and S. Bolognani,
"*A ringed–pole spm motor for sensorless drives – electromagnetic analysis, prototyping and tests*",
in IEEE International Symposium on Industrial Electronics, ISIE 2010, Bari, IT, Jul. 4–7, 2010.


A. Faggion, E. Fornasiero, N. Bianchi and S. Bolognani,
"*Sensorless capability of fractional-slot surface-mounted PM motors*",
in Electric Machines Drives Conference (IEMDC), 2011 IEEE International, 2011, pp. 593 –598

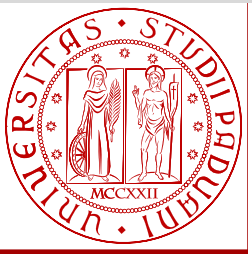

Thank you for the attention.